Fourier Reconstruction from Non-Uniform Spectral Data

Aditya Viswanathan

School of Electrical, Computer and Energy Engineering, Arizona State University
aditya.v@asu.edu

With Profs. Anne Gelb, Doug Cochran and Rosemary Renaut

Research supported in part by National Science Foundation grants
DMS 0510813 and DMS 0652833 (FRG).

Computational and Applied Mathematics Proseminar – Fall 2009
Oct 6 2009

Motivating Example

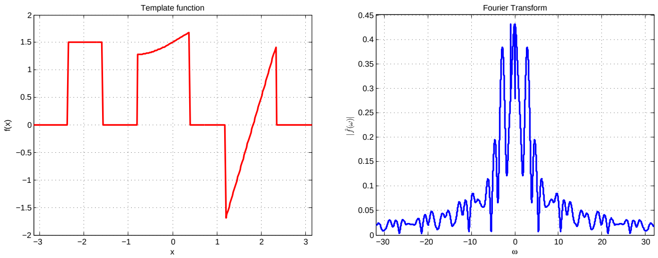

(a) Template Function (b) Fourier Transform

Figure: A motivating example

- Fourier samples violate the quadrature rule for discrete Fourier expansion
- Computational issue – no FFT available
- Mathematical issue – given these coefficients, can we/how do we reconstruct the function?
- Resolution – what accuracy can we achieve given a finite (usually small) number of coefficients?

Motivating Example

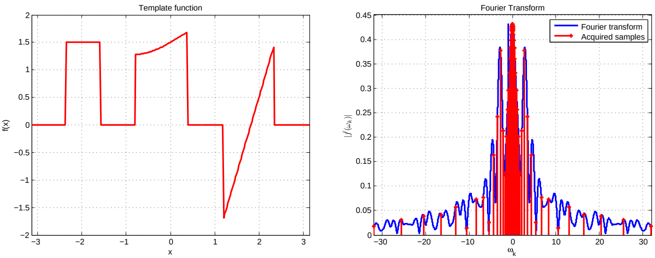

(a) Template Function (b) Fourier Coefficients, $N = 32$

Figure: A motivating example

- Fourier samples violate the quadrature rule for discrete Fourier expansion
- Computational issue – no FFT available
- Mathematical issue – given these coefficients, can we/how do we reconstruct the function?
- Resolution – what accuracy can we achieve given a finite (usually small) number of coefficients?

Motivating Example

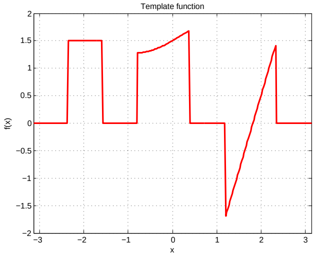

(a) Template Function

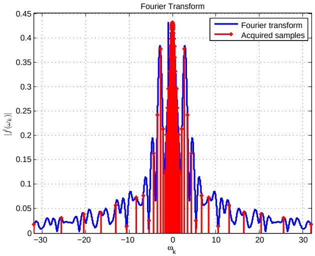

(b) Fourier Coefficients, $N = 32$

Figure: A motivating example

- Fourier samples violate the quadrature rule for discrete Fourier expansion
- Computational issue – no FFT available
- Mathematical issue – given these coefficients, can we/how do we reconstruct the function?
- Resolution – what accuracy can we achieve given a finite (usually small) number of coefficients?

Application – Magnetic Resonance Imaging

Non-Cartesian sampling trajectories have some advantages

- greater resistance to motion artifacts
- instrumentation concerns – ease in generating gradient waveforms

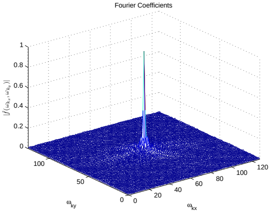

(a) Acquired Fourier Samples

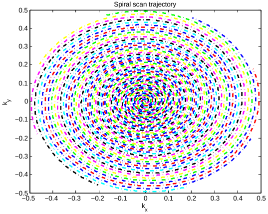

(b) Sampling Trajectory

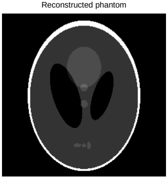

(c) Reconstructed Image

Figure: MR Imaging[a]

[a] Sampling pattern courtesy Dr. Jim Pipe, Barrow Neurological Institute, Phoenix, Arizona

In this Talk

We will discuss

- Issues with non-harmonic Fourier reconstruction
- Conventional reconstruction methods
- Accuracy vs Sampling Density
- Spectral Re-projection methods
- Incorporating edge information in the reconstruction

Outline

Problem Formulation

- Let f be defined on $\mathbb{R}$ and supported in $(-\pi, \pi)$
- It has a Fourier transform representation, $\hat{f}(\omega)$, defined as

$$\hat{f}(\omega) = \frac{1}{2\pi} \int_{-\pi}^{\pi} f(x) e^{-i\omega x} dx, \quad \omega \in \mathbb{R}$$

Objective

Recover f given a finite number of its non-harmonic Fourier coefficients,

$$\hat{f}(\omega_k), \quad k = -N, ..., N \quad \omega_k \text{ not necessarily} \in \mathbb{Z}$$

- We will refer to $\{\omega_k\}_{-N}^{N}$ as the sampling pattern/trajectory
- We will be particularly interested in sampling patterns with variable sampling density
- We will pay special attention to piecewise-smooth f

Problem Formulation

- Let f be defined on $\mathbb{R}$ and supported in $(-\pi, \pi)$
- It has a Fourier transform representation, $\hat{f}(\omega)$, defined as

$$\hat{f}(\omega) = \frac{1}{2\pi} \int_{-\pi}^{\pi} f(x) e^{-i\omega x} dx, \quad \omega \in \mathbb{R}$$

Objective

Recover f given a finite number of its non-harmonic Fourier coefficients,

$$\hat{f}(\omega_k), \quad k = -N, ..., N \quad \omega_k \text{ not necessarily} \in \mathbb{Z}$$

- We will refer to $\{\omega_k\}_{-N}^{N}$ as the sampling pattern/trajectory
- We will be particularly interested in sampling patterns with variable sampling density
- We will pay special attention to piecewise-smooth f

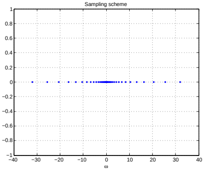

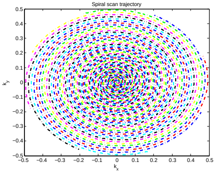

Problem Formulation

- Let f be defined on $\mathbb{R}$ and supported in $(-\pi, \pi)$
- It has a Fourier transform representation, $\hat{f}(\omega)$, defined as

$$\hat{f}(\omega) = \frac{1}{2\pi} \int_{-\pi}^{\pi} f(x) e^{-i\omega x} dx, \quad \omega \in \mathbb{R}$$

Objective

Recover f given a finite number of its non-harmonic Fourier coefficients,

$$\hat{f}(\omega_k), \quad k = -N, ..., N \quad \omega_k \text{ not necessarily} \in \mathbb{Z}$$

- We will refer to $\{\omega_k\}_{-N}^{N}$ as the sampling pattern/trajectory
- We will be particularly interested in sampling patterns with variable sampling density
- We will pay special attention to piecewise-smooth f

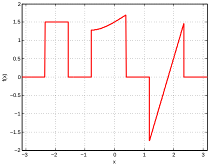

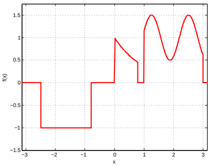

Sampling Patterns

- Jittered Sampling: $\omega_k = k \pm \tau_k, \quad \tau_k \sim U[0, \theta],\ k = -N, -(N-1), ..., N$
- Log Sampling: $|\omega_k|$ is logarithmically distributed between 10^{-v} and N, with $v > 0$ and $2N+1$ being the total number of samples.

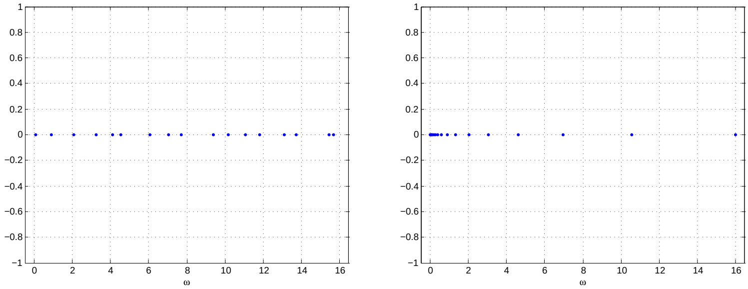

(e) Jittered Sampling (f) Log Sampling

Figure: Non-uniform Sampling Schemes (right half plane), $N = 16$

The Non-harmonic Reconstruction Kernel

- Consider standard (harmonic) Fourier reconstruction. The Fourier partial sum $S_N f(x) = \sum_{|k|\leq N} \hat{f}(k)e^{ikx}$ can be written as $S_N f(x) = (f * D_N)(x)$ where $D_N(x) = \sum_{|k|\leq N} e^{ikx}$ is the Dirichlet kernel.
- Now consider non-harmonic Fourier reconstruction using the sum $S_N \tilde{f}(x) = \sum_{|k|\leq N} \hat{f}(\omega_k)e^{i\omega_k x}$. We may again write $S_N \tilde{f}(x) = (f * A_N)(x)$ where $A_N(x) = \sum_{|k|\leq N} e^{i\omega_k x}$ is the non-harmonic kernel.
- The non-harmonic kernels do not constitute a basis for span $\{e^{ikx}, |k| \leq N\}$

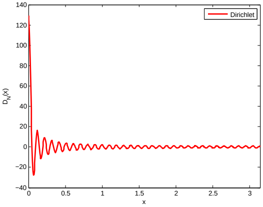

Figure: The Dirichlet Kernel plotted on the right half plane, $N = 64$

The Non-harmonic Reconstruction Kernel

- Consider standard (harmonic) Fourier reconstruction. The Fourier partial sum $S_N f(x) = \sum_{|k| \leq N} \hat{f}(k) e^{ikx}$ can be written as $S_N f(x) = (f * D_N)(x)$ where $D_N(x) = \sum_{|k| \leq N} e^{ikx}$ is the Dirichlet kernel.
- Now consider non-harmonic Fourier reconstruction using the sum $S_N \tilde{f}(x) = \sum_{|k| \leq N} \hat{f}(\omega_k) e^{i\omega_k x}$. We may again write $S_N \tilde{f}(x) = (f * A_N)(x)$ where $A_N(x) = \sum_{|k| \leq N} e^{i\omega_k x}$ is the non-harmonic kernel.
- The non-harmonic kernels do not constitute a basis for span $\{e^{ikx}, |k| \leq N\}$

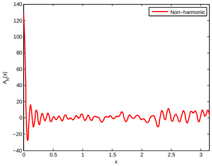

(a) Jittered Sampling

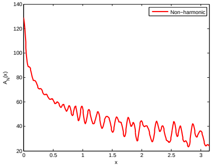

(b) Log Sampling

Figure: Non-harmonic Kernel, $N = 64$

The Non-harmonic Reconstruction Kernel

- Consider standard (harmonic) Fourier reconstruction. The Fourier partial sum $S_N f(x) = \sum_{|k| \leq N} \hat{f}(k) e^{ikx}$ can be written as $S_N f(x) = (f * D_N)(x)$ where $D_N(x) = \sum_{|k| \leq N} e^{ikx}$ is the Dirichlet kernel.
- Now consider non-harmonic Fourier reconstruction using the sum $S_N \tilde{f}(x) = \sum_{|k| \leq N} \hat{f}(\omega_k) e^{i\omega_k x}$. We may again write $S_N \tilde{f}(x) = (f * A_N)(x)$ where $A_N(x) = \sum_{|k| \leq N} e^{i\omega_k x}$ is the non-harmonic kernel.
- The non-harmonic kernels do not constitute a basis for span $\{e^{ikx}, |k| \leq N\}$

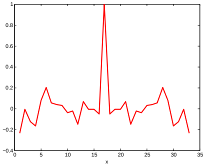

(a) Jittered Sampling

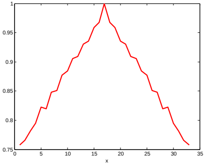

(b) Log Sampling

Figure: Autocorrelation plot of the kernels

Non-harmonic Kernels

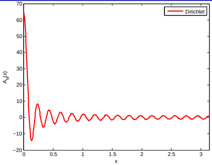

(a) Dirichlet, $N = 32$

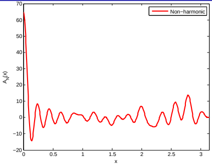

(b) Jittered, $N = 32$

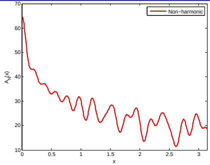

(c) Log, $N = 32$

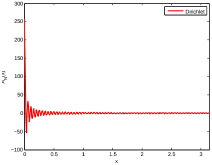

(d) Dirichlet, $N = 128$

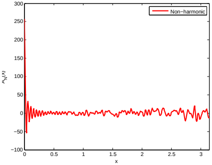

(e) Jittered, $N = 128$

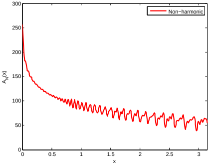

(f) Log, $N = 128$

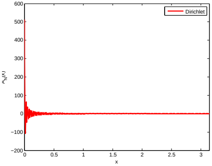

(g) Dirichlet, $N = 256$

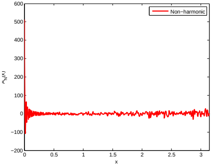

(h) Jittered, $N = 256$

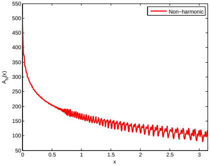

(i) Log, $N = 256$

Reconstruction Examples

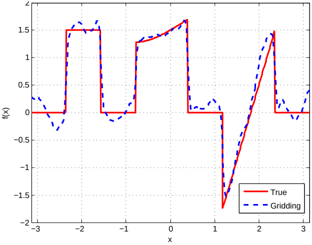

(a) "Jittered" Sampling

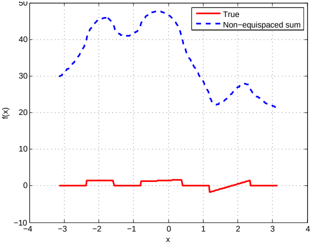

(b) "Log" Sampling

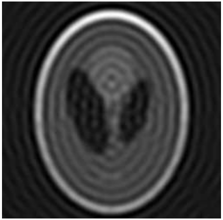

(c) "Spiral" Sampling

Figure: Non-harmonic Fourier sum Reconstruction, $N = 128$

Outline

Conventional Reconstruction Methods

Several approaches available to perform reconstruction

- Convolutional gridding – most popular
- Uniform resampling
- Iterative Methods

– "Fix" the quadrature rule while evaluating the non-harmonic sum

$$S_N \tilde{f}(x) = \sum_{k=-N}^{N} \alpha_k \hat{f}(\omega_k) e^{i\omega_k x}$$

– α_k are density compensation factors

e.g., $\alpha_k = \omega_{k+1} - \omega_k$

– Evaluated using a "non-uniform" FFT

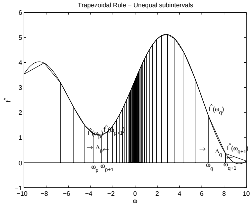

Figure: Evaluating the non-uniform Fourier sum

Although there are distinct difference in methodology and computational cost, reconstruction accuracy is similar in most schemes. We will look at convolutional gridding to obtain an intuitive understanding of the problems in reconstruction

Conventional Reconstruction Methods

Several approaches available to perform reconstruction

- Convolutional gridding – most popular
- Uniform resampling
- Iterative Methods

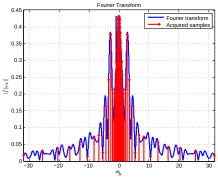

(a) Non-harmonic modes

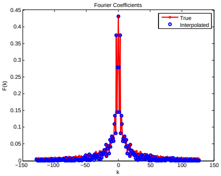

(b) Obtain uniform modes

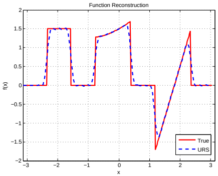

(c) (Filtered) Fourier sum

Figure: Uniform Resampling

Although there are distinct difference in methodology and computational cost, reconstruction accuracy is similar in most schemes. We will look at convolutional gridding to obtain an intuitive understanding of the problems in reconstruction

Conventional Reconstruction Methods

Several approaches available to perform reconstruction

- Convolutional gridding – most popular
- Uniform resampling
- Iterative Methods

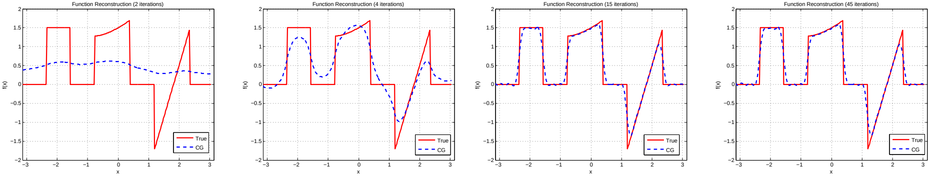

(a) after iteration 2 (b) after iteration 4 (c) after iteration 15 (d) after iteration 45

Figure: Iterative Reconstruction

Although there are distinct difference in methodology and computational cost, reconstruction accuracy is similar in most schemes. We will look at convolutional gridding to obtain an intuitive understanding of the problems in reconstruction

Conventional Reconstruction Methods

Several approaches available to perform reconstruction

- Convolutional gridding – most popular
- Uniform resampling
- Iterative Methods

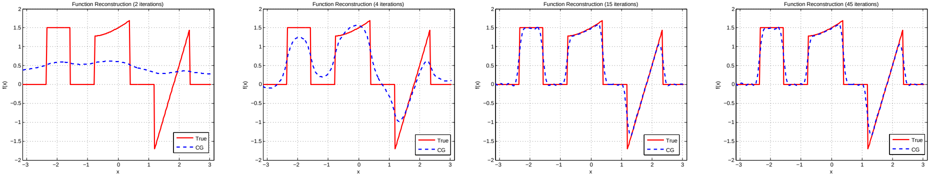

(a) after iteration 2 (b) after iteration 4 (c) after iteration 15 (d) after iteration 45

Figure: Iterative Reconstruction

Although there are distinct difference in methodology and computational cost, reconstruction accuracy is similar in most schemes. We will look at convolutional gridding to obtain an intuitive understanding of the problems in reconstruction

Convolutional Gridding

To evaluate $S_N \tilde{f}(x) = \sum_{k=-N}^{N} \alpha_k \hat{f}(\omega_k) e^{i\omega_k x}$ efficiently

1. Map the non-uniform modes to a uniform grid. A convolution operation is typically used.
2. Compute a Fourier or filtered Fourier partial sum.
3. If required, compensate for the mapping operation.

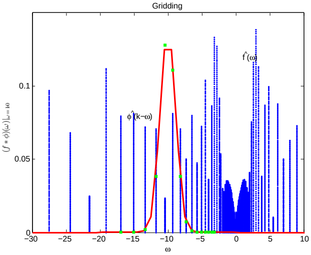

Figure: Gridding

The new coefficients on the uniform grid are therefore given by

$$\hat{f} * \hat{\phi}\Big|_{\omega=k} \approx \sum_{m \text{ st. } |k-\omega_m| \leq q} \alpha_m \hat{f}(\omega_m) \hat{\phi}(k - \omega_m)$$

Choose the interpolating function ϕ to be *essentially bandlimited*, i.e.,

$$\begin{array}{ll} \hat{\phi}(\omega) \approx 0 & |\omega| > q,\ q \in \mathbb{R}, \text{small} \\ \phi(x) \approx 0 & |x| > \pi \\ \phi(x) \neq 0 & x \in [-\pi, \pi] \end{array}$$

Convolutional Gridding

To evaluate $S_N\tilde{f}(x) = \sum_{k=-N}^{N} \alpha_k \hat{f}(\omega_k) e^{i\omega_k x}$ efficiently

1. Map the non-uniform modes to a uniform grid. A convolution operation is typically used.
2. Compute a Fourier or filtered Fourier partial sum.
3. If required, compensate for the mapping operation.

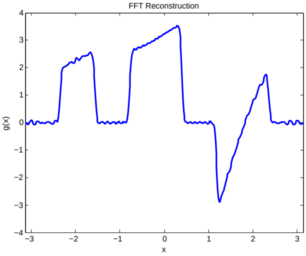

Figure: Fourier Reconstruction

The new coefficients on the uniform grid are therefore given by

$$\hat{f} * \hat{\phi}\Big|_{\omega=k} \approx \sum_{m \text{ st. } |k-\omega_m|\leq q} \alpha_m \hat{f}(\omega_m)\hat{\phi}(k-\omega_m)$$

Choose the interpolating function ϕ to be *essentially bandlimited*, i.e.,

$$\begin{array}{ll} \hat{\phi}(\omega) \approx 0 & |\omega| > q,\ q \in \mathbb{R}, \text{small} \\ \phi(x) \approx 0 & |x| > \pi \\ \phi(x) \neq 0 & x \in [-\pi, \pi] \end{array}$$

Convolutional Gridding

To evaluate $S_N \tilde{f}(x) = \sum_{k=-N}^{N} \alpha_k \hat{f}(\omega_k) e^{i\omega_k x}$ efficiently

1. Map the non-uniform modes to a uniform grid. A convolution operation is typically used.
2. Compute a Fourier or filtered Fourier partial sum.
3. If required, compensate for the mapping operation.

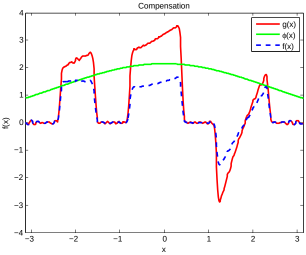

Figure: Compensation

The new coefficients on the uniform grid are therefore given by

$$\hat{f} * \hat{\phi}\Big|_{\omega=k} \approx \sum_{m \text{ st. } |k-\omega_m| \leq q} \alpha_m \hat{f}(\omega_m)\hat{\phi}(k-\omega_m)$$

Choose the interpolating function ϕ to be *essentially bandlimited*, i.e.,

$$\begin{array}{ll} \hat{\phi}(\omega) \approx 0 & |\omega| > q,\ q \in \mathbb{R}, \text{small} \\ \phi(x) \approx 0 & |x| > \pi \\ \phi(x) \neq 0 & x \in [-\pi, \pi] \end{array}$$

Convolutional Gridding

To evaluate $S_N\tilde{f}(x) = \sum_{k=-N}^{N} \alpha_k \hat{f}(\omega_k) e^{i\omega_k x}$ efficiently

1. Map the non-uniform modes to a uniform grid. A convolution operation is typically used.
2. Compute a Fourier or filtered Fourier partial sum.
3. If required, compensate for the mapping operation.

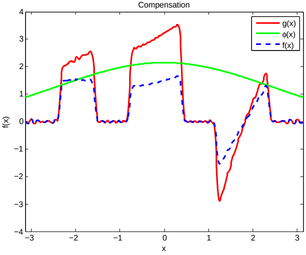

Figure: Compensation

The new coefficients on the uniform grid are therefore given by

$$\hat{f} * \hat{\phi}\Big|_{\omega=k} \approx \sum_{m \text{ st. } |k-\omega_m|\le q} \alpha_m \hat{f}(\omega_m)\hat{\phi}(k-\omega_m)$$

Choose the interpolating function ϕ to be *essentially bandlimited*, i.e.,

$$\begin{array}{ll} \hat{\phi}(\omega) \approx 0 & |\omega| > q,\ q \in \mathbb{R}, \text{small} \\ \phi(x) \approx 0 & |x| > \pi \\ \phi(x) \neq 0 & x \in [-\pi, \pi] \end{array}$$

Reconstruction Examples

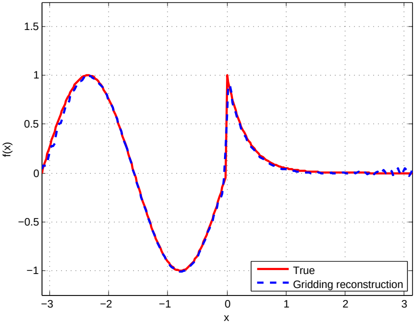

(a) Test Function reconstruction

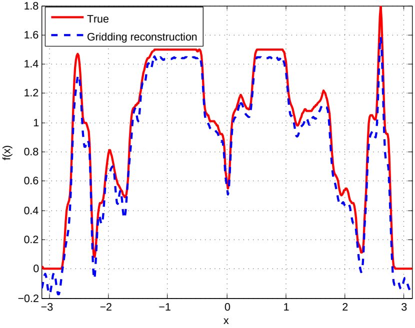

(b) Cross-section of a brain scan

Figure: Gridding reconstruction, $N = 128$ (processed by a 4^{th}-order exponential filter)

Gridding Error

Theorem (Convolutional Gridding Error)

Let $\hat{g} = \hat{f} * \hat{\phi}$ denote the true gridding coefficients and $\tilde{\hat{g}}$ denote the approximate gridding coefficients. Let Δ_k be the maximum distance between sampling points and $d_k := \frac{1}{\Delta_k}$ be the minimum sample density in the q-vicinity of k. Then, the gridding error at mode k is bounded by $e(k) \leq C \cdot \frac{1}{d_k^3}$, $k = -N, ..., N$ for some positive constant C.

Proof.

$$\hat{g}(k) - \tilde{\hat{g}}(k) = \int_{-\infty}^{\infty} \hat{f}(\omega)\hat{\phi}(k-\omega)d\omega - \sum_{p \text{ st. } |k-\omega_p| \leq q} \alpha_p \hat{f}(\omega_p)\hat{\phi}(k-\omega_p)$$

Error in approximating the integral in the interval (ω_p, ω_{p+1}) is

$$e_p = \int_{\omega_p}^{\omega_{p+1}} \hat{f}(\omega)\hat{\phi}(k-\omega)d\omega - \frac{|\omega_{p+1} - \omega_p|}{2}\left(\hat{f}(\omega_p)\hat{\phi}(k-\omega_p) + \hat{f}(\omega_{p+1})\hat{\phi}(k-\omega_{p+1})\right)$$

Gridding Error

Theorem (Convolutional Gridding Error)

Let $\hat{g} = \hat{f} * \hat{\phi}$ denote the true gridding coefficients and $\hat{\tilde{g}}$ denote the approximate gridding coefficients. Let Δ_k be the maximum distance between sampling points and $d_k := \frac{1}{\Delta_k}$ be the minimum sample density in the q-vicinity of k. Then, the gridding error at mode k is bounded by $e(k) \leq C \cdot \frac{1}{d_k^3}$, $k = -N, ..., N$ for some positive constant C.

Proof.

$$\hat{g}(k) - \hat{\tilde{g}}(k) = \int_{-\infty}^{\infty} \hat{f}(\omega)\hat{\phi}(k-\omega)d\omega - \sum_{p \text{ st. } |k-\omega_p| \leq q} \alpha_p \hat{f}(\omega_p)\hat{\phi}(k-\omega_p)$$

Error in approximating the integral in the interval (ω_p, ω_{p+1}) is

$$e_p = \int_{\omega_p}^{\omega_{p+1}} \hat{f}(\omega)\hat{\phi}(k-\omega)d\omega - \frac{|\omega_{p+1} - \omega_p|}{2}\left(\hat{f}(\omega_p)\hat{\phi}(k-\omega_p) + \hat{f}(\omega_{p+1})\hat{\phi}(k-\omega_{p+1})\right)$$

Gridding Error

Theorem (Convolutional Gridding Error)

Let $\hat{g} = \hat{f} * \hat{\phi}$ denote the true gridding coefficients and $\hat{\tilde{g}}$ denote the approximate gridding coefficients. Let Δ_k be the maximum distance between sampling points and $d_k := \frac{1}{\Delta_k}$ be the minimum sample density in the q-vicinity of k. Then, the gridding error at mode k is bounded by $e(k) \leq C \cdot \frac{1}{d_k^3}, \ k = -N, ..., N$ for some positive constant C.

Proof.

$$\hat{g}(k) - \hat{\tilde{g}}(k) = \int_{-\infty}^{\infty} \hat{f}(\omega)\hat{\phi}(k-\omega)d\omega - \sum_{p \text{ st. } |k-\omega_p| \leq q} \alpha_p \hat{f}(\omega_p)\hat{\phi}(k-\omega_p)$$

Error in approximating the integral in the interval (ω_p, ω_{p+1}) is

$$e_p = \int_{\omega_p}^{\omega_{p+1}} \hat{f}(\omega)\hat{\phi}(k-\omega)d\omega - \frac{|\omega_{p+1}-\omega_p|}{2}\left(\hat{f}(\omega_p)\hat{\phi}(k-\omega_p) + \hat{f}(\omega_{p+1})\hat{\phi}(k-\omega_{p+1})\right)$$

Gridding Error

Proof.

From trapezoidal quadrature rule error analysis

$$e_p \leq \frac{\left|\omega_{p+1} - \omega_p\right|^3 v_p}{12}$$

The total error is the error is then given by

$$\hat{g}(k) - \hat{\tilde{g}}(k) \leq \sum_p e_p \lesssim \sum_{p \text{ st. } |k-\omega_p| \leq q} e_p$$

$$\left|\hat{g}(k) - \hat{\tilde{g}}(k)\right| \leq \sum_{p \text{ st. } |k-\omega_p| \leq q} \frac{\left|\omega_{p+1} - \omega_p\right|^3 |v_p|}{12}$$

$$\leq \kappa \sum_{p \text{ st. } |k-\omega_p| \leq q} \left|\omega_{p+1} - \omega_p\right|^3, \quad \kappa = \max_p \frac{|v_p|}{12}$$

$$\leq C \cdot \Delta_k^3, \quad \text{for some positive constant } C$$

$$= C \cdot \frac{1}{d_k^3}$$

$\square$

Gridding Error

Proof.

From trapezoidal quadrature rule error analysis

$$e_p \leq \frac{\left|\omega_{p+1} - \omega_p\right|^3 v_p}{12}$$

The total error is the error is then given by

$$\hat{g}(k) - \hat{\tilde{g}}(k) \leq \sum_p e_p \lesssim \sum_{p \text{ st. } |k-\omega_p| \leq q} e_p$$

$$\begin{aligned}
\left|\hat{g}(k) - \hat{\tilde{g}}(k)\right| &\leq \sum_{p \text{ st. } |k-\omega_p| \leq q} \frac{\left|\omega_{p+1} - \omega_p\right|^3 \left|v_p\right|}{12} \\
&\leq \kappa \sum_{p \text{ st. } |k-\omega_p| \leq q} \left|\omega_{p+1} - \omega_p\right|^3, \quad \kappa = \max_p \frac{\left|v_p\right|}{12} \\
&\leq C \cdot \Delta_k^3, \quad \text{for some positive constant } C \\
&= C \cdot \frac{1}{d_k^3}
\end{aligned}$$

$\square$

Gridding Error

Proof.

From trapezoidal quadrature rule error analysis

$$e_p \leq \frac{\left|\omega_{p+1} - \omega_p\right|^3 v_p}{12}$$

The total error is the error is then given by

$$\hat{g}(k) - \hat{\tilde{g}}(k) \leq \sum_p e_p \lesssim \sum_{p \text{ st. } |k-\omega_p| \leq q} e_p$$

$$\left|\hat{g}(k) - \hat{\tilde{g}}(k)\right| \leq \sum_{p \text{ st. } |k-\omega_p| \leq q} \frac{\left|\omega_{p+1} - \omega_p\right|^3 \left|v_p\right|}{12}$$

$$\leq \kappa \sum_{p \text{ st. } |k-\omega_p| \leq q} \left|\omega_{p+1} - \omega_p\right|^3, \quad \kappa = \max_p \frac{|v_p|}{12}$$

$$\leq C \cdot \Delta_k^3, \quad \text{for some positive constant } C$$

$$= C \cdot \frac{1}{d_k^3}$$

□

Gridding Error

Proof.

From trapezoidal quadrature rule error analysis

$$e_p \leq \frac{\left|\omega_{p+1} - \omega_p\right|^3 v_p}{12}$$

The total error is the error is then given by

$$\hat{g}(k) - \hat{\tilde{g}}(k) \leq \sum_p e_p \lesssim \sum_{p \text{ st. } |k-\omega_p| \leq q} e_p$$

$$\begin{aligned}
\left|\hat{g}(k) - \hat{\tilde{g}}(k)\right| &\leq \sum_{p \text{ st. } |k-\omega_p| \leq q} \frac{\left|\omega_{p+1} - \omega_p\right|^3 \left|v_p\right|}{12} \\
&\leq \kappa \sum_{p \text{ st. } |k-\omega_p| \leq q} \left|\omega_{p+1} - \omega_p\right|^3, \quad \kappa = \max_p \frac{\left|v_p\right|}{12} \\
&\leq C \cdot \Delta_k^3, \quad \text{for some positive constant } C \\
&= C \cdot \tfrac{1}{d_k^3}
\end{aligned}$$

□

Gridding Error

Physical space reconstruction error

$$e(x) \approx g(x) - S_N\tilde{g}(x) = g(x) - S_N g(x) + S_N g(x) - S_N\tilde{g}(x)$$
$$= \underbrace{\sum_{|k|>N} \hat{g}(k)e^{ikx}}_{\text{standard Fourier truncation}} + \underbrace{\sum_{|k|\le N} \left(\hat{g}(k) - \hat{\tilde{g}}(k)\right) e^{ikx}}_{\text{gridding}}$$

- $S_N g$ suffers from Gibbs; the maximum error occurs in the vicinity of a jump (≈ 1.09 of the jump value). There is also a reduced order of convergence with $\|g - S_N g\|_2 = \mathcal{O}\left(N^{-1/2}\right)$.
- Gridding Error

$$|S_N g(x) - S_N\tilde{g}(x)| = \left|\sum_{|k|\le N} \left(\hat{g}(k) - \hat{\tilde{g}}(k)\right) e^{ikx}\right|$$
$$\le \sum_{|k|\le N} \left|\hat{g}(k) - \hat{\tilde{g}}(k)\right|$$
$$\le C \sum_{|k|\le N} \frac{1}{d_k^3}$$

Error Plots

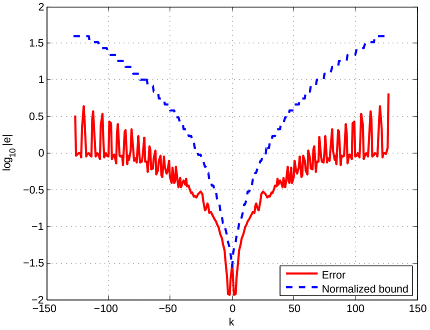

(a) Error bound, log sampling

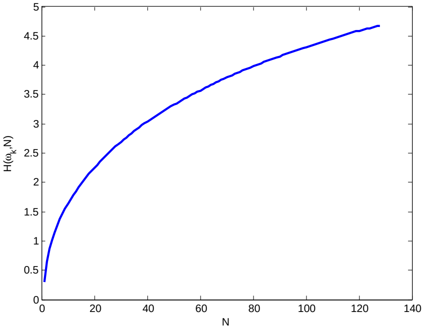

(b) $|S_N g(x) - S_N \tilde{g}(x)|$ vs N

Figure: Error Plots

Error Plots

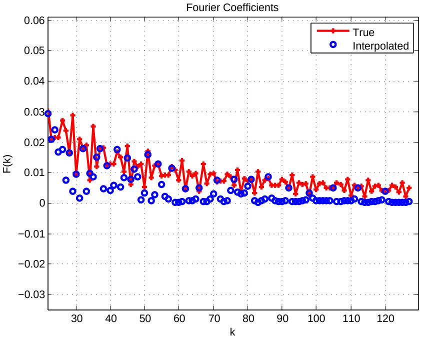

(a) Fourier coefficients – High modes

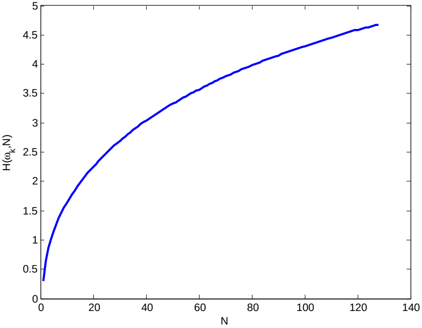

(b) $|S_N g(x) - S_N \tilde{g}(x)|$ vs N

Figure: Error Plots

Error vs Sampling Density

The reconstruction error is

$$e(x) \approx \sum_{|k|>N} \hat{g}(k)e^{ikx} + \sum_{|k|\leq N} \left(\hat{g}(k) - \hat{\tilde{g}}(k)\right) e^{ikx}$$

- 1^{st} term decreases as N increases
- 2^{nd} term increases as N increases

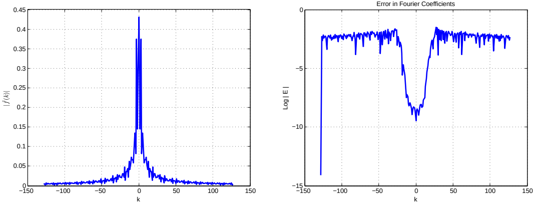

(a) Fourier coefficients (b) Coefficient error

Figure: Error in uniform re-sampling

For a given sampling trajectory and function, there is a critical value N_{crit} beyond which adding coefficients does not improve the accuracy.
While filtering decreases the error, the underlying problem is not solved.

Error vs Sampling Density

The reconstruction error is

$$e(x) \approx \sum_{|k|>N} \hat{g}(k)e^{ikx} + \sum_{|k|\leq N} \left(\hat{g}(k) - \hat{\tilde{g}}(k)\right) e^{ikx}$$

- 1^{st} term decreases as N increases
- 2^{nd} term increases as N increases

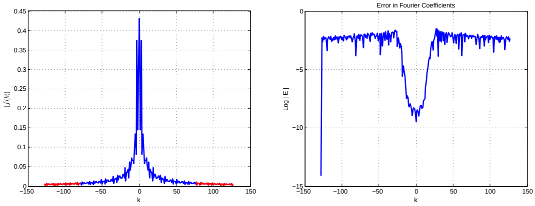

(a) Fourier coefficients (b) Coefficient error

Figure: Error in uniform re-sampling

For a given sampling trajectory and function, there is a critical value N_{crit} beyond which adding coefficients does not improve the accuracy.
While filtering decreases the error, the underlying problem is not solved.

Error vs Sampling Density

The reconstruction error is

$$e(x) \approx \sum_{|k|>N} \hat{g}(k) e^{ikx} + \sum_{|k|\leq N} \left(\hat{g}(k) - \hat{\tilde{g}}(k) \right) e^{ikx}$$

- 1^{st} term decreases as N increases
- 2^{nd} term increases as N increases

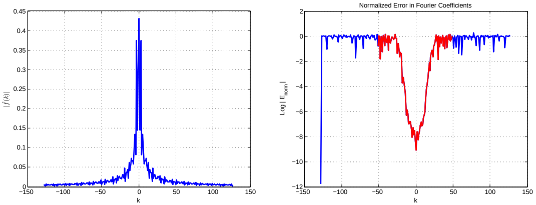

(a) Fourier coefficients (b) Coefficient error

Figure: Error in uniform re-sampling

For a given sampling trajectory and function, there is a critical value N_{crit} beyond which adding coefficients does not improve the accuracy.
While filtering decreases the error, the underlying problem is not solved.

Outline

Piecewise-Smooth Functions

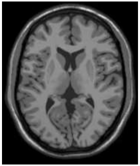

(a) Brain scan

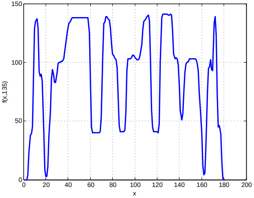

(b) Cross-section of a scan

Figure: Piecewise-smooth nature of medical images

- Due to the Gibbs phenomenon, we have non-physical oscillations at discontinuities, and, more importantly, reduced order of convergence (first order). Hence, we require a large number of coefficients to get acceptable reconstructions.
- However, by formulation of the sampling scheme and recovery procedure, the coefficients recovered at large ω are inaccurate.

$\Longrightarrow$ we need more coefficients, but the coefficients we get are inaccurate!

Spectral Re-projection

- Spectral reprojection schemes were formulated to resolve the Gibbs phenomenon. They involve reconstructing the function using an alternate basis, Ψ (known as a Gibbs complementary basis).
- Reconstruction is performed using the rapidly converging series

$$f(x) \approx \sum_{l=0}^{m} c_l \psi_l(x), \quad \text{where} \quad c_l = \frac{\langle f_N, \psi_l \rangle_w}{\|\psi_l\|_w^2},$$ f_N is the Fourier expansion of f

- Reconstruction is performed in each smooth interval. Hence, we require jump discontinuity locations
- High frequency modes of f have exponentially small contributions on the low modes in the new basis

Reducing the Impact of the High Mode Coefficients

- Filtered Fourier reconstructions

$$S_N \tilde{g}(x) = \sum_{k=-N}^{N} \sigma\left(\frac{|k|}{N}\right) \hat{g}(k) e^{ikx}$$

- Spectral re-projection

  Expansion coefficients are obtained using

$$\frac{1}{h_l^\lambda} \int_{-1}^{1} (1-\eta^2)^{\lambda-1/2} C_l^\lambda(\eta) \sum_{|k|\leq N} \hat{\tilde{g}}(k) e^{i\pi k\eta} d\eta$$

  Damping of the high modes since

$$\frac{1}{h_l^\lambda} \int_{-1}^{1} (1-\eta^2)^{\lambda-1/2} C_l^\lambda(\eta) e^{i\pi k\eta} d\eta =$$

$$\Gamma(\lambda) \left(\frac{2}{\pi k}\right)^\lambda i^l (l+\lambda) J_{l+\lambda}(\pi k)$$

  The gridding error can be shown to be

$$C' \cdot \rho(m,\lambda) \cdot \underbrace{\sum_{0<|k|\leq N} \frac{1}{d_k^3} \left(\frac{1}{|k|}\right)^\lambda}_{H(\omega_k, N, \lambda)}$$

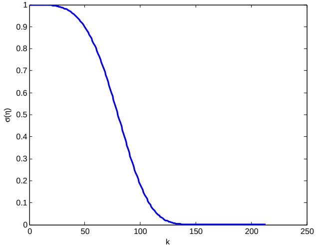

(a) Filter function

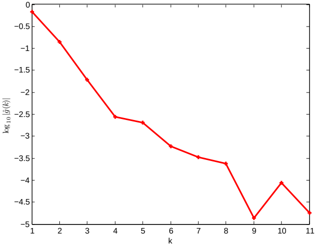

(b) Gegenbauer Coefficients

Reducing the Impact of the High Mode Coefficients

- Filtered Fourier reconstructions

$$S_N \tilde{g}(x) = \sum_{k=-N}^{N} \sigma\left(\frac{|k|}{N}\right) \hat{g}(k) e^{ikx}$$

- Spectral re-projection
  Expansion coefficients are obtained using

$$\frac{1}{h_l^\lambda} \int_{-1}^{1} (1-\eta^2)^{\lambda-1/2} C_l^\lambda(\eta) \sum_{|k|\le N} \hat{\tilde{g}}(k) e^{i\pi k\eta} d\eta$$

  Damping of the high modes since

$$\frac{1}{h_l^\lambda} \int_{-1}^{1} (1-\eta^2)^{\lambda-1/2} C_l^\lambda(\eta) e^{i\pi k\eta} d\eta = \Gamma(\lambda)\left(\frac{2}{\pi k}\right)^{\lambda} i^l (l+\lambda) J_{l+\lambda}(\pi k)$$

  The gridding error can be shown to be

$$C' \cdot \rho(m,\lambda) \cdot \underbrace{\sum_{0<|k|\le N} \frac{1}{d_k^3}\left(\frac{1}{|k|}\right)^{\lambda}}_{H(\omega_k,N,\lambda)}$$

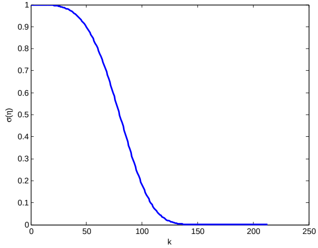

(c) Filter function

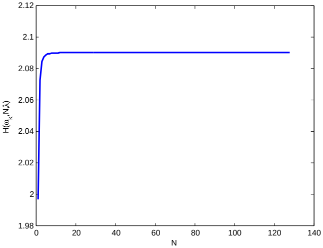

(d) $H(\omega_k, N, \lambda)$

Gegenbauer Reconstruction - Results

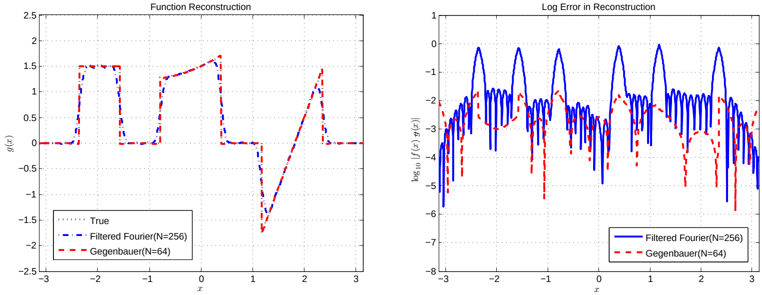

(e) Reconstruction

(f) Reconstruction error

Figure: Gegenbauer reconstruction

- Filtered Fourier reconstruction uses 256 coefficients
- Gegenbauer reconstruction uses 64 coefficients
- Parameters in Gegenbauer Reconstruction - $m = 2, \lambda = 2$

Error Plots

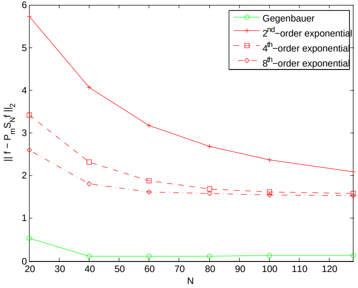

(a) 2-norm error

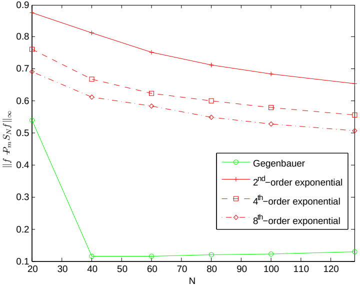

(b) Maximum-norm error

Figure: Error Plots – Filtered and Gegenbauer Reconstruction

Incorporating Edge Information

- Solve the following equation

$$\hat{f}(k) = \sum_{p \in \mathcal{P}} [f](\zeta_p) \, \frac{e^{-ik\zeta_p}}{2\pi i k}$$

- Use the concentration method on the recovered coefficients

$$S_N^{\sigma}[f](x) = i \sum_{k=-N}^{N} \hat{f}(k) \, \mathrm{sgn}(k) \, \sigma\left(\frac{|k|}{N}\right) e^{ikx}$$

- Solve for the jump function directly from the non-harmonic Fourier data

$$\begin{aligned} \min \quad & \| \, [f] \, \|_1 \\ \text{s.t.} \quad & \mathcal{F}\{[f]\}\big|_{\omega_k} = i \, \mathrm{sgn}(\omega) \, \sigma\left(\frac{|\omega|}{N}\right) \hat{f}\Big|_{\omega_k} \end{aligned}$$

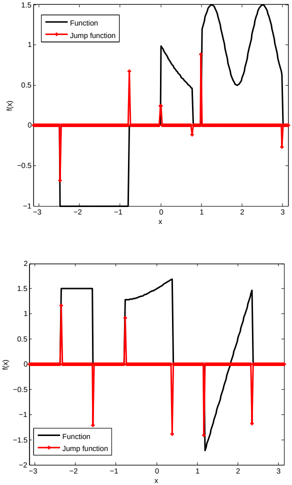

Figure: Edge Detection

Methods Incorporating Edge Information

- Compute the high frequency modes using the relation ▸ Compare

$$\hat{f}(k) = \sum_{p \in \mathcal{P}} [f](\zeta_p) \, \frac{e^{-ik\zeta_p}}{2\pi i k}$$

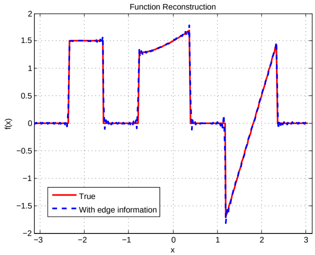

(a) Reconstruction - Using edge information

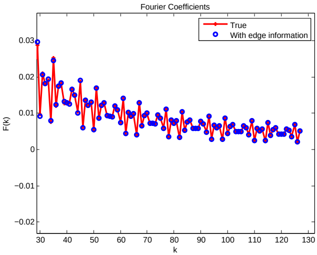

(b) The high modes - Using edge information

Figure: Reconstruction of a test function using edge information

Summary

- We introduced the Fourier reconstruction problem for non-uniform spectral data
- We discussed the inherent problems associated with non-uniform Fourier data
- We briefly looked at conventional reconstruction methods
- We studied the error characteristics and relation to sampling density
- We looked at spectral re-projection and methods incorporating edge information to obtain better reconstructions

Current Emphasis

- Incorporating edge detection into the reconstruction scheme